CORE
Metadata, citation and similar papers at core.ac.uk
Provided by Cronfa at Swansea University

Swansea University
Prifysgol Abertawe

Cronfa
Setting Research Free

Cronfa - Swansea University Open Access Repository

This is an author produced version of a paper published in :
Canadian Journal of Remote Sensing

Cronfa URL for this paper:
http://cronfa.swan.ac.uk/Record/cronfa31494

Paper:
Sutherland, G., Chasmer, L., Kljun, N., Devito, K. & Petrone, R. (2017). Using High Resolution LiDAR Data and a Flux Footprint Parameterization to Scale Evapotranspiration Estimates to Lower Pixel Resolutions. *Canadian Journal of Remote Sensing*, 0-0.
http://dx.doi.org/10.1080/07038992.2017.1291338

This article is brought to you by Swansea University. Any person downloading material is agreeing to abide by the terms of the repository licence. Authors are personally responsible for adhering to publisher restrictions or conditions. When uploading content they are required to comply with their publisher agreement and the SHERPA RoMEO database to judge whether or not it is copyright safe to add this version of the paper to this repository.
http://www.swansea.ac.uk/iss/researchsupport/cronfa-support/

Using high resolution LiDAR data and a flux footprint parameterization to scale evapotranspiration estimates to lower pixel resolutions

Research Paper

Sutherland, G.[1], L. E. Chasmer[2], N. Kljun[3], K. J. Devito[4], and R. M. Petrone[1,*]
[1]Department of Geography and Environmental Management, University of Waterloo, Waterloo, Ontario, Canada
[2]Department of Geography, University of Lethbridge, Lethbridge Alberta Canada
[3]Department of Geography, Swansea University, Swansea, United Kingdom
[4]Department of Biological Sciences, University of Alberta, Edmonton, Alberta, Canada

*Corresponding Author (rpetrone@uwaterloo.ca)

Author Contact Information
Mr. George Sutherland
Department of Geography and Environmental Management, University of Waterloo, 200 University Ave. W, Waterloo, Ontario, Canada, Tel: 519-888-4567x39185, george.sutherland@uwaterloo.ca

Dr. Laura. E. Chasmer
Department of Geography, University of Lethbridge, 4401 University Dr., Lethbridge AB, Canada, Tel: (403) 332-2016, laura.chasmer@uleth.ca

Dr. Natascha Kljun
Department of Geography, Swansea University, Swansea, United Kingdom, Tel: +44 1792 602801, n.kljun@swansea.ac.uk

Dr. Kevin Devito
Department of Biological Sciences, University of Albeta, 116 St. and 85 Ave., Edmonton, AB, Canada, Tel: 780-492-9387, kdevito@ualberta.ca

*Dr. Richard M. Petrone
Department of Geography and Environmental Management, University of Waterloo, 200 University Ave. W, Waterloo, Ontario, Canada, Tel: 519-888-4567x39175, rich.petrone@uwaterloo.ca

Abstract

Over the last several decades the hydrologically sensitive Boreal Plains ecoregion of Western Canada has experienced significant warming and drying. To better predict implications of land cover changes on evapotranspiration (ET) and future water resources in this region we used high resolution light detection and ranging and energy balance data to spatially parameterise the Penman-Monteith ET model. Within a 5 km x 5 km area of peatland ecosystems, riparian boundaries, and upland mixedwood forests, the influence of land cover heterogeneity on the accuracy of modelled ET is examined at pixel sizes of 1, 10, 25, 250, 500 and 1000 m, representing resolutions common to popular satellite products (SPOT, Landsat and MODIS). Modelled ET was compared with tower-based eddy covariance measurements using a weighted flux footprint model. Errors range from 10% to 36% of measured fluxes and results indicate that sensors with small pixel sizes (1 m) offer significantly better accuracy in large heterogeneous flux footprints, while a wider range of pixel sizes (<25 m) can be suitably applied to smaller homogeneous footprints. Mid (250 m) and coarse (>500 m) pixel sizes offered significantly less accuracy, although changes in pixel size within this range offered comparable results.

Key words: Evapotranspiration modelling; evapotranspiration scaling; LiDAR, eddy covariance; vegetation structure; Boreal.

Introduction

Climate warming is expected to have a disproportionately large impact on Canada's high latitude regions and to alter precipitation (P) and evapotranspiration (ET) patterns in Boreal Canada (IPCC, 2007). Western Canada's Boreal Plains ecozone covers approximately 629,527km^2 (National Forest Inventory, 2006) and is a hydrologically sensitive region where potential ET (PET) generally exceeds P on an annual basis, creating persistent water-deficit conditions that are interrupted by infrequent wet years occurring on a 10-15 year cycle (Devito et al., 2005a). Consequently, ET is commonly the largest component of the surface energy and water budgets during the growing season in high latitude regions (Comer et al., 2000; Cleugh et al., 2007; Raddatz et al., 2009). Therefore, an accurate understanding of ET and its driving processes is essential for characterizing water partitioning and atmospheric losses from the water balance, especially as the climate in this region continues to warm and become drier.

However, accurately assessing ET at the scales of interest to water managers is difficult due to the heterogeneous nature of this region (Ferone and Devito, 2004; Smerdon et al., 2005), the fragmented and changing land cover due to resource extraction (Lee and Boutin, 2006; Turetsky and St. Louis, 2006; Graf, 2009), and accessibility issues in largely remote locations. As a result, traditional point-scale or tower-based measurements of cumulative energy and water flux data are sparse and difficult to spatially extrapolate (Næsset and Økland, 2002; Loheide and Gorelick, 2005; Coops et al., 2007). Remote sensing offers the ability to collect information on ecosystems of interest over a variety of spatial and temporal resolutions, and has provided a platform from which point and tower data can be scaled to landscapes or regions of interest to resource managers.

Modern methods linking remote sensing with energy and water balance data take the form of surface energy balance methods, which rely on radiated thermal measurements to infer surface temperature and available energy, from which ET can be estimated as a residual (Bastiaanssen et al., 1998; Su, et al., 2002; Caparrini et al., 2003; Kustas et al., 2003; Jiang and Islam, 2006). Several popular remote sensing energy balance models that have emerged include SEBS (Su, 2002), S-SEBI (Roerink et al., 2000), SEBAL (Bastiaanssen, 1998; Ruhoff et al., 2012) and METRIC (Allen et al., 2007). Such methods are useful as they measure physical radiative properties of a surface that are directly related to ET (Overgaard et al., 2006). However, errors associated with energy balance methods can originate from small inaccuracies in measurement of surface temperature that propagate to larger errors in the estimation of turbulent fluxes (Cleugh et al., 2007).

The Penman-Monteith (PM) equation (Monteith, 1965) has also been successfully used to estimate ET across a variety of climates and land covers (Allen, 1998; Ventura 1999; Chen et al., 2005b; Cleugh et al., 2007; Armstrong et al., 2008; Leuning et al., 2008). In the context of land surface models (LSM) the PM model is often driven using energy balance and stomatal resistance datasets, which provide temporal variability of surface conditions, while remote sensing data products provide a platform to scale the model to land cover types based on average leaf area index per land cover type or per pixel (Leuning et al., 2008; Sutherland et al., 2014).

Additionally, spectral vegetation index (SVI) methods indirectly estimate ET as a function of vegetation distribution and reflectance parameters (Running and Nemani, 1988; Kite and Spence, 1995; Chen and Cihlar, 1996; Jiang and Islam, 1999; Haboudane et al., 2004; Wang et al., 2005; Pisek et al., 2011), and thus leaf area index (LAI) is the primary measure of green vegetation in SVIs that estimate ET (Wang et al., 2005). However, SVIs have been shown to saturate beyond certain LAI thresholds (Haboudane et al., 2004; Wang et al., 2005; Wu et al., 2008). Additionally, spectral reflectance values given off by understory vegetation and soil surfaces are known to introduce significant background noise in mixed pixels (Chen and Cihlar, 1996; Lim et al., 2003; Parker et al., 2001).

Both energy balance and SVI methods have been applied to many different regions and have shown promising results in most cases. There are however, several drawbacks common to both methods, particularly within heterogeneous environments: 1) Coarse resolutions can lead to landscape heterogeneity not being resolved within mixed pixels (Moran and Jackson, 1991; Hudak et al., 2002; Kustas et al., 2004; Nagler et al., 2005; McCabe and Wood, 2006; Anderson et al., 2012); 2) passive remote sensors saturate at high levels of LAI (Lüdeke et al. 1991; Haboudane et al., 2004; Wu et al., 2008) and therefore underestimate ET when applied to multi-layer, densely foliated ecosystems; 3) while they can provide information on vegetation distribution in the horizontal direction, they cannot directly sense the structure of surface vegetation in the vertical direction (Hudak et al., 2002); and 4) validation of ET estimates from coarse satellite data can be difficult due to the large disparity in scale between in situ ET measurements and modelled ET values (Li et al., 2009; Anderson et al., 2012) resulting in the inclusion of land areas not represented by the EC system for validation (Göeckede et al. 2008; Chasmer et al. 2011a).

While spectral remote sensing data provide information on the spatial characteristics of the ecosystem such as canopy cover, vegetation health, and land surface heterogeneity (Turner et al., 2002; Göckede et al., 2008), air-borne light detection and ranging (LiDAR) data go a step further by measuring the full three-dimensional characteristics of the land surface offering high resolution data products on vegetation structure (Lim and Treitz, 2004; Hopkinson et al., 2005; Morsdorf et al., 2006; Hopkinson and Chasmer, 2007; Chasmer et al., 2011b; Korhonen, et al., 2011; Hansen et al., 2014; Saito et al. 2015; Schumacher et al., 2015; and many more). Of the LiDAR data products available, vegetation height and LAI are the most relevant to estimating ET, as these parameters influence physiological, aerodynamic, and energy components of ET models.

To the authors' knowledge, few studies have used canopy structural information obtained from LiDAR data within land surface or ecosystem models to estimate ET fluxes (Neale et al., 2011; Mitchell et al., 2012), and fewer studies have integrated LiDAR data with a footprint model for the direct purpose of assessing how modelled ET differs using vegetation structure inputs of varying pixel sizes over heterogeneous land surface areas. Chasmer et al. (2011a) introduced this topic by integrating LiDAR derivatives of canopy structure with the footprint parameterization of Kljun et al. (2004) to better understand uncertainties in gross primary production (GPP) within 1 km resolution MODIS pixels. Sutherland et al. (2014) built on this work by using LiDAR-derived vegetation parameters to assess the accuracy of spatially explicit high-resolution vs bulk average model inputs to produce estimates of ET scaled beyond the tower footprint, but neither study examined a broad range of remote sensing pixel sizes. Consequently, uncertainty remains surrounding the accuracy of common sensor pixel sizes that may be used to characterize heterogeneous ecosystems within LSMs.

To examine how modelled ET varies using vegetation structure inputs at a variety of pixel sizes over heterogeneous landscapes the following study uses airborne LiDAR data products (LAI, canopy roughness) and a network of energy balance towers to parameterize the PM ET model at a pixel size of 1 m^2 within the heterogeneous Boreal Plain ecozone following methods of Chasmer et al. (2011b) and Sutherland et al. (2014). The primary objective of this study is to assess the accuracy of variable pixel sizes (1, 10, 25, 250, 500, 1000 m) as inputs to the PM ET model over homogeneous to heterogeneous land cover types in the Boreal Plains. LiDAR is used to generate 3D inputs to aerodynamic roughness and LAI. The model is then run on decreasing pixel sizes up to 1000 m and compared with eddy covariance data for validation.

The parameterization of ecosystem and land surface models using an integrated LiDAR-footprint approach at different pixel sizes may improve our understanding of the influence of spatial heterogeneity on model results at coarse resolutions, site representation of EC measurements, and discrimination of the 3D canopy characteristics required for spatial estimates of LAI and surface roughness not available using spectral remote sensing methods. This study, therefore, will quantify pixel sizes that best approximate EC estimates of ET within variable footprint extents and land cover types and offer insight into scaling methods in heterogeneous environments.

Study Site

The Utikuma Region Study Area (URSA) (Figure 1) is located 370 km north of Edmonton and is comprised of a network of research sites that have been the focus of numerous studies (e.g. Devito et al., 2005a, b; Petrone et al., 2007; Brown et al. 2010; Chasmer et al. 2011a; Petrone et al. 2011; Brown et al., 2013; Petrone et al. 2015). The URSA is characterized by a complex patchwork of heterogeneous land cover types including: mixed-wood uplands comprised of trembling aspen (*Populus tremuloides*), minimal balsam poplar (*Populus balsamifera*) and white spruce (*Picea glauca*); sparsely treed *Sphagnum* and black spruce (*Picea mariana*) peatlands; and shallow ponds with peat extension up to 40 m from the pond edge. The study area is hydrologically sensitive due to the sub-humid climate and extensive anthropogenic and natural disturbance (Lee and Boutin, 2006; Turetsky and St. Louis, 2006; Graf, 2009; Petrone et al. 2015). Mean annual temperature measured nearby at Slave Lake is 1.7 ^{o}C (1980 – 2010), while average annual precipitation is 515 mm (Petrone et al. 2007).

Two regenerating upland mixed-wood stands are examined in this study (Figure 1b). The northern stand was harvested in February of 2007, while the southern stand was harvested in February of 2008. Canopy heights determined from airborne LiDAR within these regenerating mixed-wood stands range from 0.5 m to 16 m and LAI ranges from 0 to 4. Both stands are surrounded by a mature aspen canopy between 10-20 m in height.

Figure 1: a) 5 km^2 land cover classification; b) local land cover classification surrounding energy balance and eddy covariance towers; c) 5 km^2 canopy height model (m); d) 5 km^2 digital elevation model (m above sea level); and e) 5 km^2 leaf area index map.

Materials and Methods

Hydro-meteorological instrumentation used to drive modelled ET

To inform and drive the PM model meteorological and hydrological data were collected from June 1st to August 31st, 2008, at a 5 km x 5 km study area using a network of eleven energy balance towers (Table 1) measuring ground temperature profiles (T_G, ^oC) (Omega copper-constantin, Campbell Scientific Inc, Logan, Utah, USA) at 0.1, 0.25, 0.5 and 1 m below ground; net radiation (Q*, W m^{-2}) at 3 m (NRLite, Kipp and Zonen, The Netherlands); and air temperature (T_a,^oC) and relative humidity (RH, %) at 1 and 2 m above ground (HOBO Onset Pro Temp/RH, Hoskin Scientific, Vancouver, Canada). Two energy balance towers are located each in upland mature mixed-wood forests, riparian, treed wetland and open wetland land cover types and are averaged for input into the PM model, while one tower is located over a pond.

Approximately 4000 porometry measurements of leaf stomatal conductance (g_s, mmol m^{-2} s^{-1}) were also collected throughout the study period within regenerating mixed-wood and mature aspen stands (SC-1 Decagon Devices, Inc. WA) (Giroux, 2012), coincident with EC measurements. These were averaged per species type and age class (mature, regenerating) and input into the PM model.

Table 1.

LiDAR data collection and processing

Airborne scanning LiDAR data were collected prior to foliage loss in mid-September, 2008 by Airborne Imaging Inc. and contracted by the Government of Alberta. The system used was a small footprint discrete-return ALTM 3100EA (Optech Inc.,Toronto ON), operated at a flying height of 1400 m above ground level, with a pulse repetition frequency of 50 kHz and a scan angle of ±25^{o}. A swath overlap of 50% ensured that all sides of trees and the ground surface were sampled. Data derivatives used as input into the PM model included a high resolution (1 m) digital elevation model (DEM), canopy height model (CHM), LAI, and a landcover classification (Sutherland et al., 2014; Chasmer et al. 2016).

The land cover classification divided the land surface into groups including upland forest, water, open wetland, treed wetland, and disturbance and was compared with manual delineation of wetland and water areas from aerial photos (Halsey et al. 2004) and field data collection (Chasmer et al. 2016). Errors of omission of wetland, upland forest and pond areas, which make up the dominant land cover within the 5 km x 5 km study area were manually corrected in areas where open and closed wetlands were classified as upland forest (~8% of the area).

While energy balance data was used to inform temporal variability in ET over the study period, LiDAR data products were used to inform spatial variability in ET across the 5 km x 5 km study site. Leaf area index, a data product used to estimate stomatal resistance in equation (1), was estimated from LiDAR-derived canopy gap fraction (number of ground returns divided by all returns within a column, x, y, z), and allometric estimates of canopy clumping, needle to shoot area ratio, and woody to total area ratios (Chen et al., 2006; Sutherland et al., 2014) were applied per dominant species within each land cover type.

Description of the Penman-Monteith Model to be parameterised using energy balance and LiDAR data

The PM model is described as:

$$\lambda E = \frac{[\Delta(Q* - Q_G)] + \rho_a C_p \frac{(e_s - e_a)}{r_a}}{\Delta + \Upsilon\left(1 + \frac{r_s}{r_a}\right)} \quad (1)$$

and requires temporally varying inputs of λ (latent heat of vaporization [MJ kg^{-1}]), Δ (slope of the vapour pressure curve [kPa $^oC^{-1}$]), Q* (net radiation [here as MJ m^{-2} h^{-1}]), Q_G (soil heat flux density [MJ m^{-2} h^{-1}]), ρ_a (density of the air [kg m^{-3}]), c_p (specific heat of the air [KJ kg^{-1} K^{-1}]), e_s (saturation vapour pressure [kPa]), e_a (actual vapour pressure represented as [kPa]), and ϒ (psychrometric constant [kPa $^oC^{-1}$]) measured by energy balance towers unique to each land cover type.

Following the methods of Sutherland et al. (2014) spatially explicit values of r_a (aerodynamic resistance [s m^{-1}]) and r_s (surface resistance [s m^{-1}]) were calculated for each 1 m x 1 m pixel in the study area using LiDAR-derived measurements of canopy height (CHM) and LAI, such that unique r_a and r_s were estimated for each pixel as:

$$r_a = \frac{\ln\left[\frac{(z_m - d)}{z_{om}}\right] \ln\left[\frac{(z_h - d)}{z_{oh}}\right]}{k^2 u_z} \quad (2)$$

and

$$r_s = \frac{r_l}{LAI} \quad (3)$$

where z_m is the height of wind measurements [m]; z_h is the height of humidity measurements [m]), u_z is the wind speed [m s^{-1}], and k is von Karman's constant. Roughness layers dependent on spatially varying vegetation structure were derived from LiDAR and include: d (zero plane displacement [m]) and z_o and z_{oh} (roughness length governing momentum and heat and water vapour, respectively [m]) (Oke, 1987). Bulk stomatal resistance [r_l, s m^{-1}] was determined from porometry measurements and applied to land cover types. The model outputs a spatially explicit high resolution (1 x 1 m) estimate of ET for each land cover type in the study area.

Scaling the PM model to lower resolution pixels

To determine the degree that landscape heterogeneity contributes to differences in modelled ET across a range of pixel sizes, spatially explicit estimates of cumulative daily ET at a pixel sizes of 1 m x 1 m are resampled to larger sizes characteristic of commonly available satellite data (10, 25, 250, 500, and 1000 m). A 'majority' resampling methodology in ArcGIS (ESRI, CA) was employed, whereby new ET values were assigned to each pixel based on the land cover type that comprised the majority of each larger pixel (Turner et al., 1989). All resampling is done based on original 1 m x 1 m daily ET values, as opposed to resampling from a previous aggregation (Bian and Butler, 1999; Wu, 2004).

Validating the PM model using eddy covariance measurements and a flux footprint model

Two eddy covariance (EC) systems are used to measure water fluxes for validation of modelled ET. One EC system, located 3 m above the northern regenerating stand, represents highly localised fluxes representative of the regenerating stand. A second EC system, located 22.5 m above the southern regenerating stand, represents a range of different land cover influences on ET in addition to the harvested area directly in the footprint of the EC system (due to the larger footprint size of the tower) (Figure 2). Within both regenerating aspen uplands vegetation was sparse and remained <50 cm in height, and as a result instrument height above ground surface is considered approximately equal to instrument height above the newly regenerating canopy.

Both sites were equipped with a three-dimensional sonic anemometer (CSAT 3, Campbell Scientific, AB Canada) and an open-path infrared gas analyzer (IRGA) (LI7500, LI-COR Inc., Lincoln, NE) and estimate water fluxes from ecosystems at a sampling rate of 20 Hz, averaged to half-hourly periods (Brown et al., 2010; Petrone et al., 2015). EC data were filtered for periods of low turbulence ($u^* < 0.23$ m s^{-1} based on the inflection point of u^* in relation to energy balance closure) and corrected for density effects (Webb et al., 1980; Leuning and Judd, 1996), coordinate rotation (Kaimal and Finnigan, 1994), and sensor separation (Leuning and Judd, 1996). As a final correction, energy balance closure was calculated and forced for the study period to account for any differences between turbulent fluxes and available energy (Blanken et al., 1997; Twine et al., 2000; Petrone et al., 2001; Barr et al., 2006). Following these quality control steps, approximately 35% of data was lost and subsequently gap filled using the mean over 14-day periods (Falge et al., 2001).

To validate ET modelled at varying pixel sizes (1, 10, 25, 250, 500, and 1000 m) with EC estimates at flux towers the spatial influences on temporally-varying fluxes needs to be determined. To do this, a weighted flux footprint parameterisation (Kljun et al. 2015) with a pixel size of 1 m was used to model the spatial extent of the footprint (Figure 2), such that the footprint area is used to map the probability of water (or CO_2, CH_4, etc.) flux into the atmosphere as a function of atmospheric turbulence, instrument height, wind speed, and wind direction measured during each half hourly period. .

Following Chasmer et al. (2011), weighted probability density functions (PDF) extending to 80% of the total probability were calculated every 30 minutes and summed to daily footprints.

The result is a raster grid of the spatio-temporal footprint model where each 1 m^2 pixel is assigned a weighting based on its probability to contribute a water flux to the eddy covariance measurements (Figure 2). This unique weighting for each pixel was then used as a multiplier to either increase or decrease the importance of modelled ET pixels within the footprint of the EC systems. This reduces uncertainty in the validation of modelled vs. measured fluxes because, instead of comparing EC estimates of ET (which is directional) with landscape-scale average modelled ET, this method instead applies the same directionality to the modelled fluxes (Hopkinson et al. 2016), thereby reducing comparisons with modelled values originating from other parts of the ecosystem that were not measured by EC at that point in time.

Flux footprints were eliminated for non-ideal days (i.e. during periods of poor weather, low atmospheric stability, or questionable data periods). The lower sensor height of the 3 m EC system, as well as the tall aspen canopy surrounding the tower, resulted in stable atmospheric conditions experienced more frequently relative to the tall 22.5 m tower measuring above the aspen canopy. As a result, 72 days of footprint data were available for the 22.5 m EC tower and 22 days were available for the 3 m EC tower. The extraction and validation of modelled ET within flux footprints is repeated for daily cumulative ET modelled at pixel sizes of 1, 10, 25, 250, 500, and 1000 m to determine the influence of sensor pixel size on model accuracy within heterogeneous environments. When validating ET modelled at pixel sizes >1 m^2, larger pixels were resampled to 1 m2 in order to standardize and match the number of ET pixels that were multiplied by PDF flux footprint pixels.

Figure 2: Cumulative weighted flux footprints from: a) 3m; and b) 22.5m EC towers for the study period June 1 to Aug 31.

Results

Footprint Climatology

The dominant wind direction observed at the 3 m EC tower was between 330 - 355^o, following the long axis of the north regenerating aspen upland that the tower is situated in (Figure 2a). Daily flux footprints extended up to 500 m upwind of the EC system, and footprint margins extended out of the homogeneous regenerating aspen stand approximately 60% of the time as a result of wind direction and neutral atmospheric stability. However, the probability that the point of maximum flux contribution (x_{max}) extended outside of the regenerating aspen upland remained less than 10%.

The dominant wind direction observed at the 22.5 m EC tower was between 220 - 280^o (Figure 2b). In the early half of the study period unstable atmospheric conditions resulted in smaller flux footprints for this site, extending up to 1 km from the EC tower and originating from variable wind directions, while more stable atmospheric conditions promoted larger flux footprints during the middle-to-late portion of the study period, frequently occurring from the dominant wind direction (220 - 280^o) and extending up to 3 km upwind of the tower into a variety of heterogeneous land cover types. Consequently, while the composition of the footprint surrounding the 3 m tower was relatively homogeneous, the footprint surrounding the 22.5 m tower was far more heterogeneous. Within the season-average footprint surrounding the 22.5 m tower 60% of the land area was mixed-wood aspen upland, 13% peatland, 10% pond, 12% riparian, and 5% regenerating aspen, though the contribution of each of these land cover types was highly variable from one day to the next.

Comparing modelled ET and eddy covariance methods within footprints

Cumulative measured ET in the footprint surrounding the 3 m EC tower was 54 mm over a 22-day period of measured EC data (Figure 3a). During the same period, ET modelled at a pixel size of 1 m within flux footprints totalled 60 mm, and showed no significant difference (Mann-Whitney Rank Sum Test, $p>0.05$) from measured ET (Table 2). Increasing pixel sizes of modelled ET to 10 or 25 m resulted in little change in agreement with measured ET. At pixel sizes of 10 and 25 m modelled ET overestimated measured ET by 8 mm (14%) and 9 mm (15%), respectively, and neither size showed a significant difference (Mann-Whitney Rank-Sum Test, $p>0.05$) with measured ET. Increasing pixel size to 250 m results in a 16 mm (30%) overestimation when modelled ET was compared to measured ET. A similar trend is observed when pixel size was increased to 500 and 1000 m, where both of these pixel sizes overestimate measured ET by 20 mm (36%) (Figure 4).

Figure 3: Eddy covariance measured ET and cumulative ET estimated at each pixel size and extracted from flux footprints surrounding the: a) 3m EC tower; and b) 22.5m tower.

Cumulative measured ET at the 22.5 m EC tower was 164 mm over a 72-day period of measured (Figure 3b). Over the same period cumulative ET modelled at a 1 m pixel size was 180 mm and overestimated measured ET by 16 mm (10%). Significant differences (Mann-Whitney Rank Sum Test, $p<0.05$) were observed between ET modelled at a pixel size of 1 m and measured values (Table 3). Increasing pixel size of modelled ET to 10 and 25 m resulted in overestimates of 31 mm (19%) and 34 mm (20%), respectively, relative to measured ET in the footprint surrounding the 22.5 m tower (Figure 4). Increasing pixel sizes further to 250, 500, and 1000 m yields similar results to those observed within the 3 m EC footprint, where these pixels are frequently larger than the land cover types within the flux footprint, and in some cases are larger than the footprint itself (Figure 4).

Table 2

Table 3

Figure 4: residual between eddy covariance ET measurements at the 3 m and 22.5 m EC towers relative to ET modelled at pixel sizes of 1, 10, 25, 250, 500, and 1000 m.

Scaling and assessing errors in ET estimates beyond the tower footprint

As estimates of ET at a pixel size of 1 m proved to be closest to measured ET within the flux footprints of both validation towers, these 1 m estimates were used as a basis to assess error in modelled ET when scaled to the 5 km x 5 km study site (i.e. outside of EC flux footprints). At a pixel size of 1 m cumulative modelled ET for the 5 km study area ranged between 151 - 239 mm with an average of 162 ± 50 mm (Table 4), of which 62% was from mature aspen forests, 16% was from treed peatlands, 9% was from riparian zones, 8% was from open peatlands, 5% was from ponds, and 1% was from regenerating aspen stands (Table 5). Over a 90 day modelling period, the greatest ET rates were observed in mature upland aspen stands (216 mm average) and ponds (210 mm average) while lowest ET was observed in riparian (158 mm average) areas and recently harvested regenerating aspen stands (151 mm average).

The greatest spatial variability in modelled ET, as indicated by the range in standard deviations for ET modelled within each land cover type, was seen at land cover boundaries where sharp transitions exist in canopy structure (Figure 5a). The influence of edges was assessed by examining average ET (+/- standard deviation) within 10 m of edges compared to ET rates in the center of large land covers such as mature aspen stands and large ponds. Variability in modelled ET within 10 m of edges was, on average, 20-30% greater than ET modelled at the center of large land covers. Higher than average variability in ET was also evident in rough or patchy canopies which promote turbulent mixing. This was most pronounced in peatlands and transitional riparian zones (Figure 5a) where a uniform canopy is not present and standard deviations of ET values were twice as large as those observed in mature and regenerating forested uplands.

Table 4.

Table 5.

Figure 5: ET estimates for the 5 km x 5 km study site at pixel sizes of: a) 1 m ; b) 10 m ; c) 25 m ; d) 250 m ; e) 500 m; and f) 1000 m.

Increasing the pixel size of modelled ET to 10 and 25 m resulted in site-scale average ET increasing to ~165 mm (Table 4) with subtle (+/- 1%) changes in the contribution of each land cover to total ET in the study area (Table 5), where boundaries of smaller land covers such as treed peatlands and riparian zones were misclassified as adjacent open peatlands and ponds (Figure 6ba,b). These changes in land cover contribution to total ET were coincident with a

~17% decline in site-wide variability (standard deviation) of modelled ET at 10 and 25 m pixel sizes, relative to 1 m values (Figure 5b,c).

Further increasing the pixel size of modelled ET to 250 m resulted in site-scale average ET increasing to 167 ± 39 mm and a 21% decline in the spatial variability of ET relative to 1 m values. The decline in ET heterogeneity across the study site is reflected in the contribution of each land cover to total ET (Table 5), particularly in regenerating aspen stands which are underestimated by 38% relative to regenerating aspen ET values modelled at a pixel size of 1 m. ET modelled in ponds and treed peatlands is underestimated by 6 and 8%, respectively, and ET from open peatlands is overestimated by 10% (Figure 6c) relative to 1 m values in each of these land cover types. Additionally, while maximum ET (ET_{max}) rates of 450 mm were evident when modelled using a pixel size of 1 m, ET_{max} was 320 mm when modelled at a pixel size of 250 m due to the loss of edges.

Increasing the pixel size of modelled ET to 500 m results in a site-scale average ET estimate of 171 ± 36 mm and a 28% decline in the spatial variability of ET relative to 1 m values. At a pixel size of 500 m the contribution of each land cover to the site-average ET is significantly different relative to 1 m values, where ET from ponds and open peatlands is overestimated by 102 and 150%, respectively, and ET from treed peatlands, riparian zones, and regenerating aspen stands are underestimated by 52, 100, and 100 %, respectively (Table 5).

There were similar results for 1000 m pixels, where the spatial variability in ET is underestimated by 79% relative to 1 m values. Riparian zones and regenerating aspen stands are eliminated (Figure 5f) from the landscape, while treed peatlands are underestimated by 75% and ponds and open peatlands are overestimated by 160 and 114%, respectively, relative to values at a pixel size of 1 m in each of these land cover types (Table 5).

Figure 6: Difference in cumulative ET estimates between 1m x 1m ET estimates and ET estimated at pixel sizes of: a) 10 m; b) 25 m; c) 250 m; d) 500 m; and e) 1000 m. Blue pixels indicate where resampled pixels overestimate 1 m ET estimates; red pixels indicate where resampled pixels underestimate 1 m ET estimates.

Discussion

Modelled ET within Eddy Covariance Footprints

ET estimated at a pixel size of 1 m were most similar to measured ET at the 3 m and 22.5 m towers, and were comparable to ranges of uncertainty found at other study sites using high (Loheide and Gorelick, 2005) and low (Cleugh et al., 2007; Li et al., 2008) resolution ET models. For a given pixel size, stronger agreement was observed between measured and modelled ET in smaller footprints because the footprint was more likely to be comprised of a single homogeneous land cover type. This is observed at the 3 m EC tower where x_{max} remained within the northern regenerating aspen upland for ~90% of the study period and measurements from the EC system are characterized by a homogeneous land cover which is suitably resolved using 1, 10, and 25 m pixel sizes. Small declines in accuracy observed with 10 and 25 m pixels are due to the partial loss of edges surrounding the regenerating stand which enhance turbulence and promote ET. Larger footprints, however, extend in to a variety of land covers with variable ET regimes, resulting in contamination and uncertainty in observations between measured and modelled ET for a given pixel size. This is observed at the 22.5 m tower, where the flux footprint extends up to 3 km into a variety of land cover types and ET estimated at a pixel size of 10 m are significantly different and disagree with measured ET by 19%.

Regardless of how homogeneous a flux footprint is, the ability to utilize remote sensing platforms to accurately predict ET is largely dependent on a sensor's ability to resolve canopy structural characteristics, landscape distribution, and landscape edges. Consequently, ET modelled at the finest pixel size provided the closest agreement with measured ET, as 1 m pixel estimates were able to suitably represent the same vegetation structural characteristics that were driving ET measured at the EC system. This is particularly important in narrow land covers such as riparian zones and fragmented wetlands which serve as corridors between larger forest patches (O'Neill et al., 1996) and often play a crucial role in characterizing the regional water balance (Kimball et al., 1999; Chen et al., 2007). As pixel size increases, pixels become larger than the areal extent of land cover patches and vegetation structural characteristics are generalized, resulting in a loss of landscape heterogeneity and a decline in the spatial variability of ET estimates (Turner et al., 1989; O'Neill et al., 1996; Kustas and Norman, 2000; Kustas et al., 2004; Nagler et al., 2005; McCabe and Wood, 2006; Li et al., 2008). Wu et al., (2004) observed similar results in Boreal regions where the number of landscape patches followed a decreasing trend as pixel size declined.

Such declines in heterogeneity result in overestimations of ET in the western Boreal Plains as small land cover types are misclassified as the spatially dominant aspen uplands, which are characterized by a greater LAI and higher ET rates relative to the ponds, peatlands, and riparian zones which they eliminate from the landscape at larger pixel sizes. This was observed in modelled results with the elimination of riparian zones and regenerating aspen uplands from the landscape at pixel sizes of 500 and 1000 m. Additionally, depending on the fragmented nature of a heterogeneous landscape, thresholds can be crossed beyond which variable sensor resolutions yield static results, as was evident where ET estimates at pixel sizes of 500 and 1000 m are identical within flux footprints of both EC towers due to pixel size being larger than the areal extent of the land cover patches within the flux footprint.

Land cover edge effects, which are an important contributor to measured ET in heterogeneous landscapes due to step changes in air flow (Oke, 1987; Liu et al., 1996), also become increasingly generalized as pixel size increases (Wu et al., 2004). The influence of edges, which may be manifested as stand-alone shrubs within regenerating aspen stands to sharp transition zones between land cover types, are observed within this study and often represent ET_{max} within a land cover type. As a result, the accuracy of modelled ET sharply declines when the pixel size becomes larger than individual patches of vegetation found within land cover types (O'Niell et al. 1996; Kustas et al. 2004) and, although modelled ET rates were observed to overestimate measured ET with increasing pixel size, ET_{max} declines from 450 to 186 mm (Table 4) when scaling from 1 to 1000 m resolutions as edges are generalized at landcover boundaries. Although this is particularly pronounced in heterogeneous landscapes such as the western Boreal Plains, McCabe and Wood (2006) noted a similar trend in decreasing variability and accuracy of latent heat fluxes when scaling from 120 m to 1020 m pixels in heterogeneous agricultural watersheds. Ershadi et al. (2013) also noted changes in roughness lengths around land cover borders at large (>240 m) pixel sizes and found increasingly coarse pixels to underestimate latent heat fluxes by up to 15% with the SEBS model. Consequently, the areal extent of the smallest land cover unit of interest must be taken into consideration when choosing a suitable pixel size for modelling initiatives. O'Neill et al. (1996) note that pixel size should be 2 to 5 times smaller than the smallest feature of interest, and the current study confirms these findings.

Identifying sensor resolutions appropriate for heterogeneous environments

Evaluating incremental shifts in the accuracy of changing pixel sizes provides insight into threshold responses of sensors within varying footprint compositions. The most pronounced shift in accuracy associated with a change in sensor is observed at different pixel sizes depending on the heterogeneity of the flux footprint. Within homogeneous footprints (e.g. those surrounding the 3 m EC tower) the most pronounced shift in the accuracy of modelled ET was observed when pixel size was changed from 25 to 250 m, suggesting that 1, 10, and 25 m pixels can suitably represent the vegetation structural parameters driving ET within the homogeneous footprint. Contrary to this, the most pronounced shift in the accuracy of modelled ET within heterogeneous footprints (e.g. those surrounding the 22.5 m tower) was observed when pixel size was changed from 1 to 10 m as well as from 25 to 250 m. Because the significantly larger and more heterogeneous footprint surrounding the 22.5 m tower extends up to 3 kilometers into a variety of land cover types characteristic of this region, small changes in pixel size can have pronounced implications on the ability of models to appropriately characterize vegetation structural characteristics and land cover edges.

Switching between mid (250 m) and coarse (500-1000 m) pixel sizes resulted in less pronounced changes in the accuracy of modelled ET, suggesting that within this range users of remote sensing data may not experience statistically significantly better results from using 250 m data over 500 or 1000 m data within heterogeneous landscapes, as each of these pixel sizes are unable to suitably characterize vegetation structural characteristics influencing ET. This is particularly true of 500 and 1000 m data, which showed no difference in the accuracy of modelled ET between pixel sizes relative to EC data. Such results indicate that ET predictions in heterogeneous environments benefit from utilizing the finest pixel remote sensing data available, while larger pixels can be suitably applied to homogeneous environments, although the "best" pixel size is largely contextual and dependent on the spatial extent of homogeneity in the area of interest (Wu et al., 2004; Zhao et al., 2015).

Conclusions

ET estimates at pixel sizes of 1 m x 1 m were scaled to increasingly coarse sizes (10, 25, 250, 500, 1000 m) characteristic of commonly available remote sensing data products. The objective was to determine the accuracy of ET estimates derived from a variety of pixel sizes within a heterogeneous environment. Comparison with measured EC data demonstrated that, within flux footprints, 1 m ET estimates were the most accurate and subsequent scaling to larger pixels lead to decreased accuracy due to the misrepresentation of land cover types and boundaries when pixel size is larger than the fragments of land cover types within a pixel. Mixed-wood aspen uplands dominate the western Boreal Plains landscape and are fragmented by relatively small ponds, peatlands, and riparian zones. Consequently, increasing pixel size results in the loss of ET heterogeneity as these relatively small land cover types are outweighed and misclassified as the spatially-dominant mixed-wood aspen uplands, resulting in a net overestimation of ET.

The results of this study demonstrate the benefit of using datasets with the smallest pixel size available within biogeochemical and/or land surface models applied to heterogeneous environments. Often times, ecosystems are not entirely homogeneous and are becoming increasingly fragmented. While two-dimensional (spectral) datasets provide some indication of foliage area at a snap-shot in time, three-dimensional datasets acquired using LiDAR provide additional information on canopy roughness and the impacts of ecosystem boundaries on fluxes. This will no doubt become important for planning and land use monitoring in northern regions where increased warming will exacerbate the sensitivity of ecosystems to drought (Michaelian et al. 2011).

Acknowledgements

The authors would like to thank Mr S. Brown for his technical assistance in the field. Funding for this work was provided by an NSERC Discovery Grant (Petrone), NSERC Collaborative Research and Development Grant (HEAD2), NSERC Research Tools and Instrument Grant (Petrone) and the Cumulative Environmental Managers Association (CEMA).

References

Antonarakis, A.S., J. W. Munger and P. Moorcroft. 2014. Imaging Spectroscopy- and Lidar-derived Estimates of Canopy Composition and Structure Improve Predictions of Forest Carbon Fluxes and Ecosystem Dynamics, *Geophysical Research Letters*. 41(7): 2535-2542.

Baldocchi, D. D., R. J. Luxmoore, and J. L. Hatfield. 1991. Discerning the forest from the trees: an essay on scaling canopy stomatal conductance. *Agricultural and Forest Meteorology*. 54:197-226.

Baldocchi, D., Finnigan, J.J., Wilson, K., Paw U, K.T., Falge, E. (2000). On measuring net ecosystem carbon exchange over tall vegetation on complex terrain. *Boundary-Layer Meteorol.* 96,257–291

Barcza, Z., A. Kern, L. Haszpra, N. Kljun, 2009: Spatial Representativeness of Tall Tower Eddy Covariance Measurements Using Remote Sensing and Footprint Analysis. *Agricultural and Forest Meteorology*, 149, 795-807.

Barr A.G., Morgenstern K., Black T.A., McCaughey J.H., Nesic Z. 2006. Surface energy balance closure by the eddy covariance method above three boreal forest stands and implications for the measurement of CO2 flux. *Agriculture and Forest Meteorology*, 140:322-337.

Bian, L. and R. Butler. 1999. Comparing effects of aggregation methods on statistical and spatial properties of simulated spatial data. *Photogrammetric Engineering & Remote Sensing*, 65(1), 73-84.

Blanken P.D., Black T.A., Yang P.C., Neumann H.H., Staebler R., Nesic Z., den Hartog G., Novak M.D., Lee X.. 1997. The energy balance and canopy conductance of a boreal aspen forest: partitioning overstory and understory components. *Journal of Geophysical Research* 102: 915–927.

Brown, S. M., R. M. Petrone, C. Mendoza and K. J. Devito. 2010. Surface vegetation controls on evapotranspiration from a sub-humid Western Boreal Plain wetland. *Hydrological Processes*, 24, 1072-1085.

Brown S. M., R. M. Petrone, L. Chasmer, C. Mendoza, M. S. Lazerjan, S. M. Landhäusser, U. Silins, J. Leach and K. J. Devito. 2013. *Hydrological Processes* DOI: 10.1002/hyp.9879

Brümmer, C., T. A. Black, R. S. Jassal., N. J. Grant, D. L. Spittlehouse, B. Chen, Z. Nesic, B.D. Amiro, M. A. Arian, A. G. Barr, C. P-A Bourque, C. Courselle, A. L. Dunn, L. B. Flanagan, E. R. Humphreys, P. M. Lafleur, H. A. Margolis, J. H McCaughey, and S. C. Wofsy. (2012). How climate and vegetation type influence evapotranspiration and water use efficiency in Canadian forest, peatland and grassland ecosystems. *Agricultural and Forest Meteorology*, 153, 14-30.

Chasmer, L., N. Kljun, A. Barr, A. Black, C. Hopkinson, H. McCaughey, and P. Treitz. 2008. Vegetation structural and elevation influences on CO_2 uptake within a mature jack pine forest in Saskatchewan, Canada, *Canadian Journal of Forest Research*, 38, 2746–2761, doi:10.1139/X08-121.

Chasmer, C. Hopkinson, A. Barr, A. Black, H. McCaughey, and P. Treitz, 2009. Scaling and assessment of GPP from MODIS using a combination of airborne lidar and eddy covariance measurements over jack pine forests. *Remote Sensing of Environment,* 113:82-93.

Chasmer, L., N. Kljun, C. Hopkinson, S. Brown, T. Milne, K. Giroux, A. Barr, K. Devito, I. Creed, and R. Petrone. 2011a, Characterizing vegetation structural and topographic characteristics sampled by eddy covariance within two mature aspen stands using lidar and a flux footprint model: Scaling to MODIS, *J. Geophys. Res.,* 116, G02026, doi:10.1029/2010JG001567.

Chasmer, L., R. Petrone, S. Brown, C. Hopkinson, C. Mendoza, J. Diiwu, W. Quinton, and K. Devito, 2011b, Sensitivity of modelled evapotranspiration to canopy characteristics within the Western Boreal Plain, Alberta. C. Neale and R. Gerber (eds.) *IAHS Red Book.* September 25, 2010. Jackson Hole, WY. 4 pgs.

Chasmer, L., J. Montgomery, C. Hopkinson. A morphological/vegetation structural wetland classification for Boreal Alberta, Canada. *Canadian Journal of Remote Sensing.* Special Issue on Advanced Forest Inventory. (in press). http://dx.doi.org/10.1080/07038992.2016.1196583

Chen, J.M., Cihlar, J. 1996. Retrieving leaf area index of boreal conifer forests using Landsat TM images. *Remote Sensing Environment* 55 (2), 153–162

Chen, J.M.,J. Liu, J. Cihlar, M.L. Goulden. 1999. Daily canopy photosynthesis model through temporal and spatial scaling for remote sensing applications. *Ecological Modelling,* 124, pg 99-119.

Chen JM, Govind A, Sonnentag O, ZhangY, BA, Amiro B. 2006. Leaf area index measurements at Fluxnet-Canada forest sites. *Agricultural and Forest Meteorology* 140: 257–268. doi:10.1016/j.agrformet. 2006.08.005.

Chen, B., J.M. Chen, G. Mo, et al. 2007. Modelling and scaling coupled energy, water, and carbon fluxes based on remote sensing: An application to Canada's Landmass. *J. Hydrometeor*. 8:123-143.

Cleugh, H. A., R. Leuning, Q. Mu, and S. W. Running. 2007. Regional evaporation estimates from flux tower and MODIS satellite data. *Remote sensing of Environment*, 106, 285-304.

Cressie, N. A. 1993. <u>Statistics for Spatial Data.</u> Wiley, New York.

Devito K. J., Creed I. F., and Fraser C. J. D. 2005a. Controls on runoff from a partially harvested aspen-forested headwater catchment, Boreal Plain, Canada. *Hydrological Processes* 19, 3–25.

Devito, K., I. Creed, T. Gan, C. Mendoza, R. Petrone, U. Silins, and B. Smerdon. 2005b. A framework for broad-scale classification of hydrologic response units on the Boreal Plain: is topography the last thing to consider? *Hydrological Processes*, 19, 1705- 1714.

El Maayar, M., J. M. Chen, and D. T. Price, 2008. On the use of field measurements of energy fluxes to evaluate land surface models. *Ecological Modelling*. 214:293-304.

Eriksson, H. M., L. Eklundh, A. Kuusk, and T. Nilson. 2006. Impact of understory vegetation on forest canopy reflectance and remotely sensed LAI estimates. *Remote Sensing of Environment*, 103, 408-418.

Ershadi, A., M.F. McCabe, J.P. Evans, J.P. Walker. 2013. Effects of spatial aggregation on the multi-scale estimation of evapotranspiration. *Remote Sensing of Environment*, 131, 51-62.

Falge E, Baldocchi D, Olson R, Anthoni P, Aubinet M, Bernhofer C, Burba G, Ceulemans R, Clement R, Dolman H, Granier A, Gross P, Grünwald T, Hollinger D, Jensen N-O, Katul G, Keronen P, Kowalski A, Lai CT, Law BE, Meyers T, Moncrieff J, Moors E, Munger JW, Pilegaard K, Rannick Ü, Rebmann C, Suyker A, Tenhunen J, Tu K, Verma S, Vesala T, Ilson K, Wofsy S. 2001. Gap filling strategies for long term energy flux data sets. *Agricultural and Forest Meteorology,* 107: 71–77

Foken, T. and Leclerc, M. Y. 2004. Methods and limitations in validation of footprint models. *Agr. Forest Meteorol.,* 127: 223–234.

Gelybó, G., Z. Barcza, A. Kern, N. Kljun, 2013: Effect of Spatial Heterogeneity on the Validation of Remote Sensing Based GPP Estimations, *Agricultural and Forest Meteorology*, 174-175, 43-53.

Giroux K. 2012. Pre- and Post-Harvest Carbon Dioxide Fluxes from an Upland Boreal Aspen (Populus tremuloides) Forest in Western Boreal Plain, Alberta, Canada. Masters Thesis. Wilfrid Laurier University.

Göckede, M., C. Rebmann, and T. Foken. 2004. A combination of quality assessment tools for eddy covariance measurements with footprint modelling for the characterisation of complex sites. *Agricultural and Forest Meteorology*, 127, 175-188.

Göeckede, M., T. Foken, M. Aubinet, M. Aurela, J. Banza, C. Bernhofer, J.M. Bonnefond, Y. Brunet, A. Carrara, R. Clement, E. Dellwik, J. Elbers, W. Eugster, J. Fuhrer, A. Granier, T. Grünwald, B. Heinesch, I.A. Janssens, A. Knohl, R. Koeble, T. Laurila, B. Longdoz, G. Manca, M. Marek, T. Markkanen, J. Mateus, G. Matteucci, M. Mauder, M. Migliavaca, S. Minerbi, J. Moncrieff, L. Montagnani, E. Moors, J.-M. Ourcival, D. Papale, J. Pereira, K. Pilegaard, G. Pita, S. Rambal, C. Rebmann, A. Ridrigues, E. Rotenberg, M.J. Sanz, P. Sedlak, G. Seufert, L. Siebicke, J.F. Soussana, R. Valentini, T. Vesala, H. Verbeeck, D. Yakir. 2008. Quality control of CarboEurope flux data – Part 1: Coupling footprint analyses with flux data quality assessment to evaluate sites in forest ecosystems. *Biogeosciences*, *5(2)*:433-450.

Graf, Martha D. 2009. Literature review on the Restoration of Alberta's Boreal Wetlands: Affected by Oil, Gas and In Situ Oil Sands Development. Edmonton, AB: Ducks Unlimited.

Haboudane, D., J. R. Miller, E. Pattey, P. J. Zarco-Tejada, I. B. Strachan. 2004. Hyperspectral vegetation indices and novel algorithms for predicting green LAI of crop canopies: Modeling and validation in the context of precision agriculture. *Remote Sensing of Environment*, 90(3), pp.337-352.

Halsey, L.A., D. H. Vitt, D. Bellman, S. Crow, S. Meheicic, and R. Wells. 2004. Alberta Wetland Inventory Classification System Version 2.2. ISBN No. 0-7785-2324-1 (On-line Edition)

Hansen A. J., Phillips L. B., Dubayah R., Goetz S., and Hofton M. 2014. Regional-scale application of lidar: Variation in forest canopy structure across the southeastern US. *Forest Ecology and Management*, 329: 214-226.

Heinsch, F. A., Zhao, M., Running, S. W., Kimball, J. S., Nemani, R. R., Davis, K. J., et al. 2006. Evaluation of remote sensing based terrestrial productivity from MODIS using regional tower eddy flux network observations. *IEEE Transactions on Geoscience and Remote Sensing,* 44(7), 1908−1925.

Hopkinson, C. A., and L. Chasmer. (2007). Using Discrete Laser pulse return Intensity to Model canopy Transmittance. *The Photogrammetric Journal of Finland*, 20(2), 16-27.

Hopkinson, Chasmer, L., A. Barr, N. Kljun, T. A. Black and J. H. McCaughey. 2016. Monitoring forest biomass and carbon storage by integrating airborne laser scanning and eddy covariance data. *Remote Sensing of Environment.* 181:82-95.

Jin, Z., Tian, Q., Chen, J. M., and Chen, M. 2007. Spatial scaling between leaf area index maps of different resolutions. *Journal of Environmental Management*, 85, 628−637.

Kaimal JC, Finnigan J. 1994. *Atmospheric Boundary Layer Flows: Their Structure and Measurement*. Oxford Univ. Press: New York; 255–261.

Kalma, J.D., McVicar, T.R., McCabe, M.F. 2008. Estimating land surface evaporation: a review of methods using remotely sensed surface temperature data. *Surv. Geophys*. 29, 421–469.

Kimball, J. S., S. W. Running, and S. S. Saatchi. 1999. Sensitivity of boreal forest regional water flux and net primary production simulations to sub-grid-scale land cover complexity. *J. Geophys. Res*., 104, 27 789–27 802.

Kim, J., Q. Guo, D. D. Baldocchi, M. Y. Leclerc, L. Xu, and H. P. Schmid. 2006. Upscaling fluxes from tower to landscape: Overlaying flux footprints on high-resolution (IKONOS) images of vegetation cover. *Agricultural and Forest Meteorology*. 136:132-146.

Kljun, N., P. Calanca, M. W. Rotach, and H. P. Schmid. 2004. A simple parameterisation for flux footprint predictions. *Boundary-Layer Meteorology*, 112, 503-523.

Kljun, N., P. Calanca, M. W. Rotach, and H. P. Schmid . 2015. A simple two-dimensional parameterisation for Flux Footprint Prediction (FFP). *Geoscientific Model Development*, 8, 3695–3713, 2015

Kustas, W. P. and J.M. Norman. 2000. Evaluating the Effects of Subpixel Heterogeneity on Pixel Average Fluxes. *Remote Sensing of Environment*, 74: 327-324.

Kustas, W. P., F. Li, T. J. Jackson, J. H. Prueger, J. I. MacPherson, and M. Wolde. 2004. Effects of remote sensing pixel resolution on modeled energy flux variability of croplands in Iowa. *Remote Sensing of Environment*, 535-547.

Kustas, W.P., M. C. Anderson, A. N. French, D. Vickers. 2006. Using a remote sensing field experiment to investigate flux-footprint relations and flux sampling distributions for tower and aircraft-based observations. *Advances in Water Resources*, 29:355-368.

Lee, P. and S. Boutin. 2006. Persistence and developmental transitions of wide seismic lines in the western Boreal Plains of Canada. *Journal of Environmental Management,* 78, 240-250.

Leuning R, JuddMJ. 1996. The relative merits of open and closed path analysers for measurement of eddy fluxes. *Global Change Biology* 2: 241–253.

Leuning, R., Y. Q. Zhang, A. Rajaud, H. Cleugh, and K. Tu. (2008). A simple surface conductance model to estimate regional evaporation using MODIS leaf area index and the Penman-Monteith equation. Water Resources Research, 44, W10419, doi:10.1029/2007WR006562, 2008

Li, F., W.P. Kustas, M.C. Anderson, et al. 2008. Effect of remote sensing spatial resolutions on interpreting tower-based flux observations. *Remote Sens. Environ.*, 112:337-349.

Lim, K., P. Treitz, M. Wulder, B. St-Onge and M Flood. 2003. LiDAR remote sensing of forest structure. *Progress in Physical Geography*, 27(1), 88-106.

Lindsay, J., I. F. Creed, and F. D. Beall. 2004. Drainage basin morphometrics for depressional landscapes. *Water Resources Research.* 40, W09307, doi:1029/2004WR003322.

Liu, J., J.M. Chen, T.A. Black, and M.D Novak. 1996. E-ε modelling of turbulent air flow downwind of a model forest edge. *Boundary Layer Meteorology*, 77 (1), 21-44

Loheide, S. P. and S. M. Gorelick. 2005. A local-scale, high-resolution evapotranspiration mapping algorithm (ETMA) with hydroecological applications at riparian meadow restoration sites. *Remote Sensing of Environment*, 98, 182-200.

Lüdeke, M., Janecek, A., & Kohlmaier, G. H. 1991. Modelling the seasonal CO2 uptake by land vegetation using the global vegetation index. *Tellus*, 43B, 188– 196.

Massman, W. J. and Lee, X. 2002. Eddy Covariance Flux Corrections and Uncertainties in Long- Term Studies of Carbon and Energy Exchanges. *Agric. For. Meteorol.* 113, 121–144.

McCabe M.F. and E. F. Wood. 2006 Scale influences on the remote estimation of evapotranspiration using multiple satellite sensors. *Remote Sensing of Environment* 105:271–295.

Michaelian, M., E. H. Hogg, R. J. Hall, and E. Arsenault, 2011. Massive mortality of aspen following severe drought along the southern edge of the Canadian boreal forest. *Global Change Biology.* 17(6):2084-2094.

Mitchell P. J., Lane P. N. J., and Benyon R. G. 2012. Capturing within catchment variation in evapotranspiration from montane forests using LiDAR canopy profiles with measured and modelled fluxes of water. *Ecohydrology*, 5: 708-720.

Monteith, J.L. 1965. Evaporation and environment. *In Symposium of the Society for Experimental Biology, The State and Movement of Water in Living Organisms*, Fogg GE (ed.) Vol. 19. Academic Press, Inc.: NY; 205–234.

Næsset, E., and Økland, T. 2002. Estimating tree height and tree crown properties using airborne scanning laser in a boreal nature reserve. *Remote Sens. Environ.* 79: 105–115.

Nagler, P. J. Cleverly, E. Glenn, D. Lampkin, A. Huete, Z. Wan. 2005. Predicting riparian evapotranspiration from MODIS vegetation indices and meteorological data. *Remote Sensing of Environment*, 94, 17-30.

Neale, C. M. U., Geli H., Taghvaeian S., Masih A., Pack R. T., Simms R. D., Baker M., Milliken J. A., O'Meara S., and Witherall A. J. 2011. Estimating Evapotranspiration of Riparian Vegetation using High resolution Multispectral, Thermal Infrared and Lidar Data. *Remote Sensing for Agriculture, Ecosystems, and Hydrology*, vol 81740, doi:10.1117/12.903246.

Oke TR. 1987. Boundary Layer Climates. Methuen & Co, Ltd.

O'Neill R.V., Hunsaker C.T., Timmins S.P., Timmins B.L., Jackson K.B., Jones K.B., Riitters K.H. and Wickham J.D. 1996. Scale problems in reporting landscape pattern at the regional scale. *Landscape Ecology* 11: 169–180.

Petrone R.M., Waddington J.M., Price J.S.. 2001. Ecosystem scale evapotranspiration and net CO2 exchange from a restored peatland. *Hydrological Processes* 15: 2839–2845.

Petrone, R. M., U. Silins, and K. J. Devito. (2007). Dynamics of evapotranspiration from a riparian pond complex in the Western Boreal Forest, Alberta, Canada. Hydrologocial Processes, 21, 1391-1401.

Petrone, R. M., Solondz D. S., Macrae M. L., Gignac D., and K. J. Devito. 2011. Microtopographical and canopy cover controls on moss carbon dioxide exchange in a western Boreal Plain peatland. Ecohydrology, 4, 115-129.

Petrone, R. M., L. Chasmer, C. Hopkinson, U. Silins, S. Landhausser, N. Kljun, K. J. Devito, 2015. Effects of harvesting on CO_2 and H_2O Fluxes during wet and dry years in an aspen dominated Western Boreal Plain Forest. *Canadian Journal of Forest Research*. 45:87-100.

Pitman, A.J. 2003.The evolution of, and revolution in, land surface schemes designed for climate models. *Int. J. Climatol.* 23, 479–510

Running S. W., Ramakrishna R. Nemani, David L. Peterson, Larry E. Band, Donald F. Potts. Lars L. Pierce, Michael A. Spanner. 1989. Mapping regional forest evapotranspiration and photosynthesis by coupling satellite data with ecosystem simulation. *Ecology*, 70 (4), 1090-1101.

Saito, T., Yamamoto, K., Komatsu, M., Matsuda, H., Yunohara, S., Komatsu, H., Tateishi, M., Xiang, Y.,Otsuki, K., and Kumagai, T. 2015. Using airborne LiDAR to determine total sapwood area for estimating stand transpiration in plantations. *Hydrol. Process.,* 29: 5071–5087. doi:10.1002/hyp.10482.

Saxton KE, Rawls WJ, Romberger JS, Papendick RI. 1986. Estimating generalized soil-water characteristics from texture. *Soil Science Society of America Journal* 50(4): 1031–1036.

Schmid, H. P. 1994. Source areas for scalars and scalar fluxes, *Boundary Layer Meteorology*, 67, 293–318, doi:10.1007/BF00713146.

Schumacher, J. and Christiansen, J. R. Forest canopy water fluxes can be estimated using canopy structure metrics derived from airborne light detection and ranging (LiDAR). 2015. *Agricultural and Forest Meteorology*, 203: 131-141

Sellers, P., F.G. Hall, R.D. Kelly, et al., (1997). BOREAS in 1997: experiment overview, scientific results, and future directions. *J. Geophys. Res.*, 102:28731-28769.

Sutherland, G., L.E. Chasmer, R.M. Petrone, N. Kljun, and K.J. Devito. 2014. Evaluating the use of spatially varying versus bulk average 3D vegetation structural inputs to modelled evapotranspiration within heterogeneous land covers. *Ecohydrology, In Press,* DOI 10.1002/eco.1447

Treitz, P. and P. Howarth. 2000. High spatial resolution remote sensing data for forest ecosystem classification: An examination of spatial scale. *Remote Sensing of Environment.* 72:268-289.

Treitz, P. 2001. Variogram analysis of high spatial resolution remote sensing data: An examination of boreal forest ecosystems. *International Journal of Remote Sensing.* 22(18):3895-3900.

Turetsky, M.R. and V.L. St. Louis. 2006. Disturbance in boreal peatland. R.K. Wieder and D.H. Vitt, editors. *Boreal peatland ecosystems*. Springer- Verlag, Berlin, Germany.

Turner, M. G., R. V. O'Niell, R. H. Gardner, and B. T. Milne. 1989. Effects of changing spatial scale on the analysis of landscape pattern. *Landscape Ecology*, 3, 153-162.

Turner, D. P., Gower, S. T., Cohen,W. B., Gregory, M., & Maiersperger, T. K. 2002. Effects of spatial variability in light use efficiency on satellite-based NPP monitoring. *Remote Sensing of Environment*, 80, 397−405.

Turner, D. P., Ollinger, S., & Kimball, J. 2004. Integrating remote sensing and ecosystem process models for landscape- to regional-scale analysis of the carbon cycle. *BioScience*, 54(6), 573−584.

Twine T.E., Kustas W.P., Norman J.M., Cook D.R., Houser P.R., Meyers T.P., Prueger J.H., Starks P.J., Wesely M.L.. 2000. Correcting eddy-covariance flux underestimates over a grassland. *Agricultural and Forest Meteorology* 103: 279–300.

Wang, Q., S. Adiku, J. Tenhunen, and A. Granier. 2005. On the relationship of NDVI with leaf area index in a deciduous forest site. *Remote Sensing of Environment*, 94, 244–255.

Webb EK, Pearman G, Leuning R. 1980. Correction of flux measurements for density effects due to heat and water vapour transfer. *Quarterly Journal of the Royal Meteorology Society* 106: 85–100.

Williams, M., A.D. Richardson, M. Reichstein, et al. 2009. Improving land surface models with FLUXNET data. *Biogeosci.* 6:1341-1359.

Wu, J. 2004. Effects of changing scale on landscape pattern analysis: scaling relations. *Landscape Ecology*, 19, 125-138.

Xu, S., Chen, J. M., Fernandes, R., & Cihlar, J. 2004. Effects of subpixelwater area fraction on mapping leaf area index and net primary productivity in Canada. *Canadian Journal for Remote Sensing*, 30, 797−804.

Zhang K., Kimball J.S., Mu Q., Jones L. A., Goetz S.J, W. Running S. W. 2009. Satellite based analysis of northern ET trends and associated changes in the regional water balance from 1983 to 2005. *Journal of Hydrology,* 379: 92‑110.

Zhao, G., Siebert, S., Enders, A., Rezaeil, E., Yan, C., and Ewart F. 2015. Demand for multi-scale weather data for regional crop modeling. *Agricultural and Forest Meteorology* 200: 156-171. doi:10.1016/j.agrformet.2014.09.026.

List of Symbols

λ = latent heat of vaporization [MJ kg^{-1}]

Δ = slope of the vapour pressure curve [kPa $^{o}C^{-1}$]

ρ_a = density of the air [kg m^{-3}]

Υ = psychrometric constant [kPa $^{o}C^{-1}$]

Table 1: Type of tower, instrument height above ground surface, dominant vegetation, areal coverage, mean leaf area index (LAI) and standard deviation, and mean cumulative ET for each dominant land cover type in the study area. ET values are modelled using spatially explicit 1 m x 1 m vegetation structural characteristics and measured hydro-meteorologic parameters associated with each land cover (see model description in text).

Tower type	**Instrument height (m)**	**Landcover**	**Number of Towers**	**Dominant species**	**Coverage (%)**	**LAI**	**Mean ET (mm)**
Eddy covariance	3	Upland regeneration	*1*	*Populus balsamifera L, Salix* spp., *Amelanchier alnifolia, Rosa acicularis, Viburnum edule, Cornus Canadensis, Epilobium angustifolium, Calamagrostis canadensis*	1	0.36 (1.23)	151.43
Eddy covariance	22.5	Upland regeneration	*1*				
Energy balance	3	Upland regeneration	*2*				
Energy balance	3	Mature mixedwood	*2*	*Populus tremuloides, Populas balsamifera Rosa acicularis*	58	1.40 (2.08)	216.05
Energy balance	3	Riparian	*2*	*Populus balsamifera, Picea marianca, Populus tremuloides, Betula papyrifera*	11	1.20 (1.11)	157.92
Energy balance	3	Treed peatland	*2*	*Picea marianca, Sphagnum spp.*	8	2.01 (3.16)	184.08
Energy balance	3	Open Peatland	*2*	*Sphagnum spp.*	17	0.10 (0.60)	198.02
Energy balance	3	Pond	*1*	*See text.*	5	N/A	209.83

Table 2: Difference between cumulative modelled ET at each pixel size within PDF flux footprints and eddy covariance data for all days with suitable atmospheric stability to calculate PDF flux footprints at the 3 m northern tower. Statistical differences determined using the Mann-Whitney Rank-Sum Test with a 95% confidence interval.

Resolution	**Modelled ET (mm)**	**Overestimation (mm)**	**Overestimation (%)**	**Significant Difference from EC?**	
Measured	54.48	--	--	--	--
1m	60.31	5.83	10.71	No	N = 22, p = 0.484, r2 = 0.602
10m	62.09	7.61	13.97	No	N = 22, p = 0.283, r2 = 0.611
25m	62.72	8.24	15.13	No	N = 22, p = 0.170, r2 = 0.625
250m	70.86	16.38	30.07	Yes	N = 22, p = 0.002, r2 = 0.749
500m	74.00	19.52	35.83	Yes	N = 22, p < 0.001, r2 = 0.566
1000m	74.00	19.52	35.83	Yes	N = 22 p < 0.001, r2 = 0.603

Table 3: Difference between cumulative modelled ET at each pixel size within PDF flux footprints and eddy covariance data for all days with suitable atmospheric stability to calculate PDF flux footprints at the 22.5 m southern tower. Statistical differences determined using the Mann-Whitney Rank-Sum Test with a 95% confidence interval.

Resolution	**Modelled ET (mm)**	**Overestimation (mm)**	**Overestimation (%)**	**Significant Difference from EC?**	
Measured	164.61	--	--	--	--
1m	180.29	16.29	9.93	Yes	N = 72; $p<0.001$, $r^2 = 0.206$
10m	195.31	31.31	19.09	Yes	N = 72; $p<0.001$, $r^2 = 0.201$
25m	198.28	34.28	20.90	Yes	N = 72; $p<0.001$, $r^2 = 0.201$
250m	212.17	48.17	29.37	Yes	N = 72; $p<0.001$, $r^2 = 0.213$
500m	224.70	60.70	37.01	Yes	N = 72; $p<0.001$, $r^2 = 0.275$
1000m	224.70	60.70	37.01	Yes	N = 72; $p<0.001$, $r^2 = 0.275$

Table 4: Average ET ± standard deviation, and maximum ET modelled at each pixel size for the 5 km x 5 km study area.

Resolution	Average ET (mm)	Standard Deviation (mm)	Maximum (mm)
1m	161.53	50.02	450
10m	165.59	41.34	352
25m	165.3	41.89	345
250m	167.43	39.49	320
500m	171.40	35.93	314
1000m	176.00	10.69	186

Table 5: Percent contribution of each land cover type to total landscape ET at each pixel size for the 5 km x 5 km study site.

Land Cover	**1m**	**10m**	**25m**	**250m**	**500m**	**1000m**
Pond	5.23	5.26	5.25	4.94	10.57	13.60
Open Peatland	7.98	8.08	8.02	8.83	19.96	17.11
Treed Peatland	15.62	15.69	15.81	14.37	7.42	3.98
Riparian	8.69	8.67	8.63	8.61	0.00	0.00
Regenerating	0.60	0.60	0.60	0.38	0.00	0.00
Mature mixed-wood	61.87	61.74	61.69	62.88	62.05	65.32

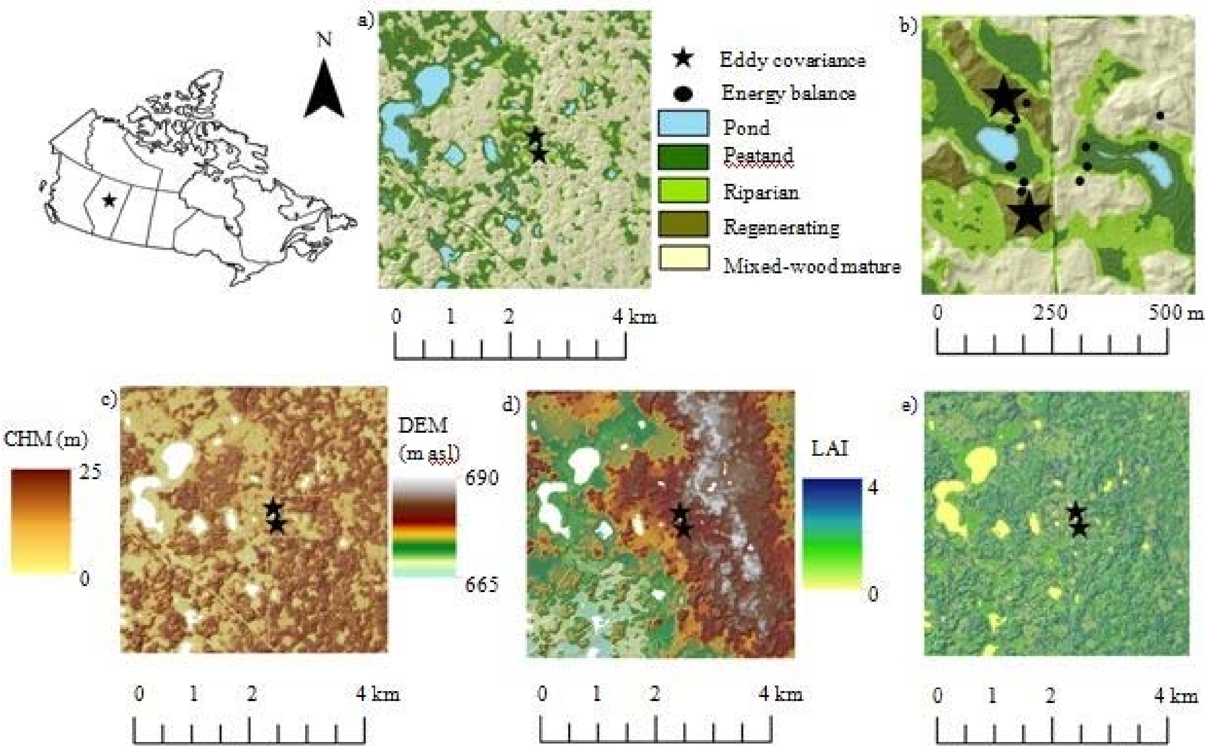

Fig. 1

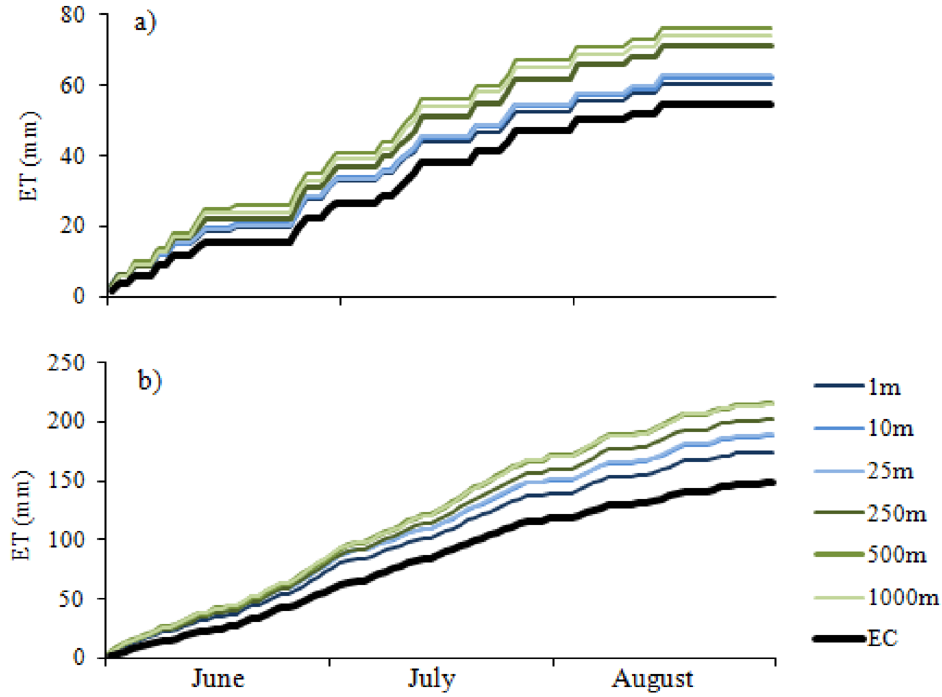
a)
b)
ET (mm)
0
20
40
60
80
0
50
100
150
200
250
June
July
August
1m
10m
25m
250m
500m
1000m
EC

Fig. 2

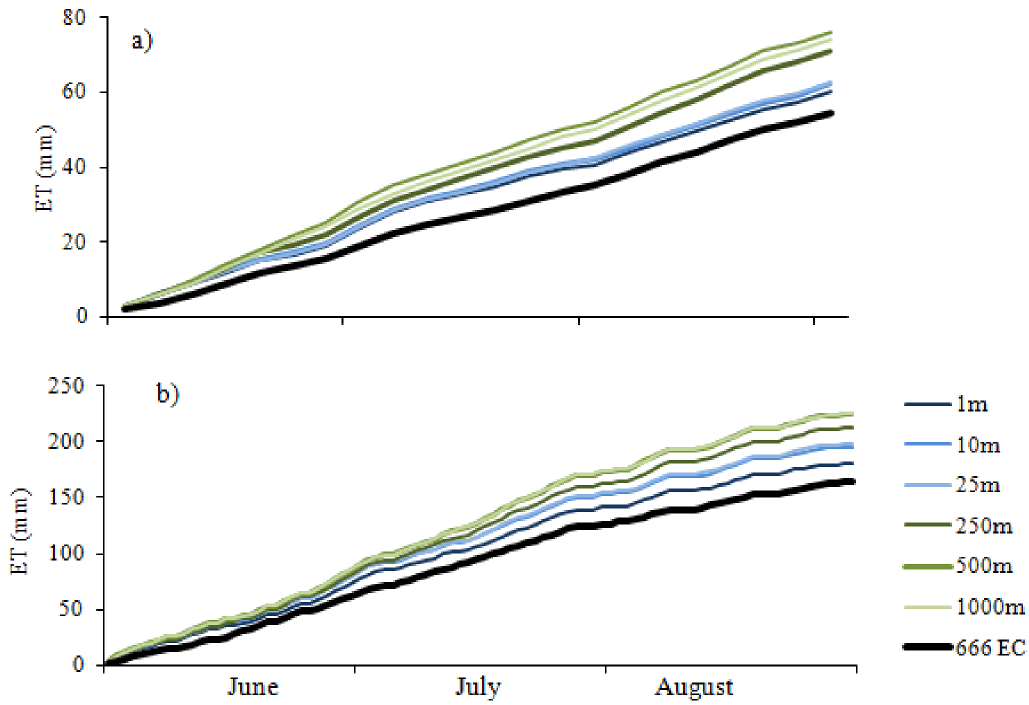
a)
b)
ET (mm)
0
20
40
60
80
0
50
100
150
200
250
June
July
August
1m
10m
25m
250m
500m
1000m
666 EC

Fig. 3

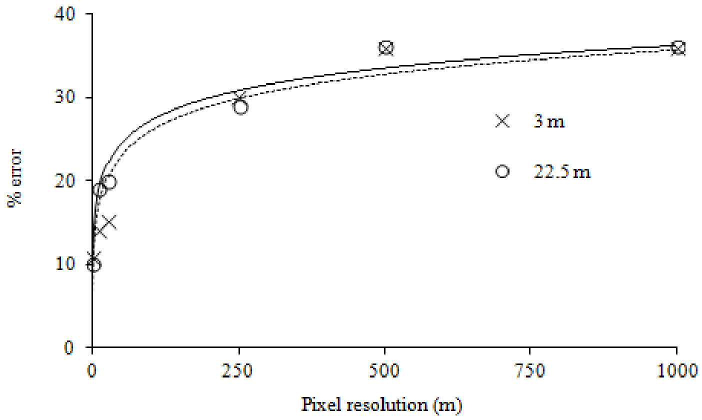
40
30
20
10
0
% error
0
250
500
750
1000
Pixel resolution (m)
3 m
22.5 m

Fig. 4

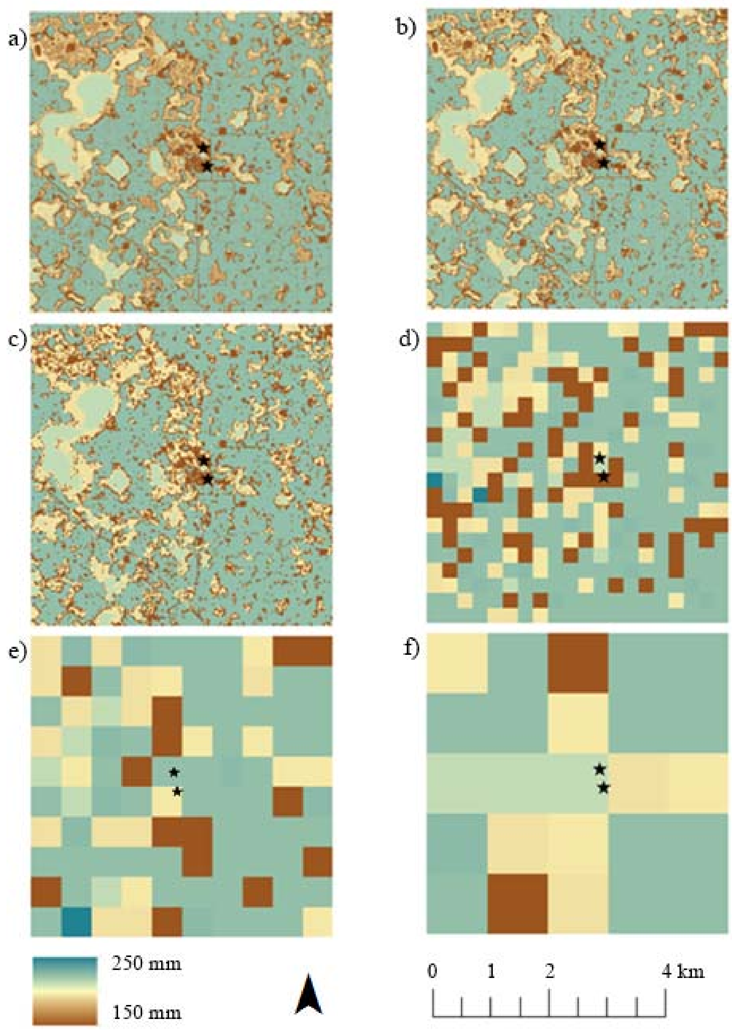
a)
b)
c)
d)
e)
f)
250 mm
150 mm
0
1
2
4 km

Fig. 5

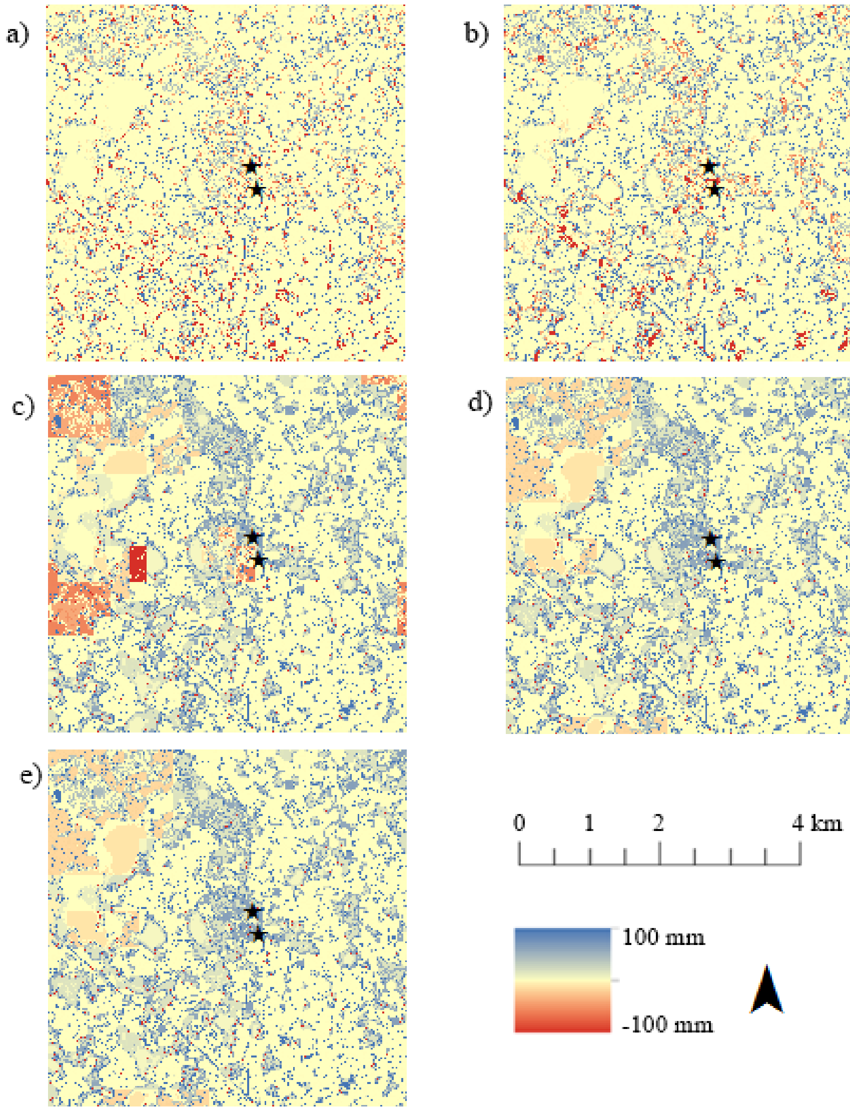

943
944 Fig. 6